Self-consistent coupling of the three-dimensional fluid turbulence code TOKAM3X and the kinetic neutrals code EIRENE

D.-M. Fan[1*] | Y. Marandet[1] | P. Tamain[2] | H. Bufferand[2] | G. Ciraolo[2] | Ph. Ghendrih[2] | E. Serre[3]

[1]PIIM, Aix-Marseille Univ., CNRS, Marseille, France
[2]IRFM, CEA, St. Paul-lez-Durance, France
[3]M2P2, Aix-Marseille Univ., CNRS, Marseille, France

***Correspondence**
D.-M. Fan, PIIM, Aix-Marseille Univ., CNRS, Marseille F-13397, France.
Email: dong-mei.fan@univ-amu.fr

Funding Information
This research was supported by the A*MIDEX project KFC, ANR-11-IDEX-0001-02. Euratom research and training programme (H2020 EURATOM), 633053. project Equip@Meso, ANR-10-EQPX-29-01.

The three-dimensional (3D) turbulence code TOKAM3X-EIRENE, coupling the 3D non-isothermal version of TOKAM3X to the EIRENE Monte Carlo solver has been developed with the ability to simulate self-consistently the interactions between large-scale flows and turbulence both in limited and diverted plasmas, including recycling. This is especially important for diverted plasmas, where neutrals play a key role and where the recycling source is strongly dominant. The code package relies on the same interface as the Soledge2D-EIRENE code, which retains state-of-the-art plasma–wall interaction, as well as atomic and molecular physics. In this paper, we present the first results obtained in WEST divertor geometry, in laminar mode, with the aim of verifying the new code package. The divertor density regimes are recovered, and the code results are shown to be consistent with the results of the two-point model, thus opening the way for turbulent simulations.

KEYWORDS
density regimes, edge plasma transport, numerical modelling

1 | INTRODUCTION

Particle and power exhaust, that is, the removal of the helium ash and the fusion power without damage to the reactor itself, specifically its plasma-facing components (PFCs), is a key issue for next-step devices. The control of the deposited heat flux and erosion at the divertor target plates is a major issue for the design and operation of next-step, high-power, long-pulse devices such as the International Thermonuclear Experimental Reactor (ITER).[1]

Heat flux calculations presently rely on transport codes, which are a combination of two-dimensional (2D) fluid codes for charged particles and a kinetic Monte Carlo code modelling the neutral species behaviour as well as their interaction with the background plasma (e.g., SOLPS,[2] SOLEDGE2D-EIRENE,[3,4] EDGE2D[5]). All these codes solve mean-field equations in which the gradient diffusion hypothesis is applied to model turbulent fluxes.[6] However, so far the anomalous transport coefficients introduced through this procedure are not consistently calculated, and are simply taken as the input parameters of the simulations. When used to interpret experiments, these transport coefficients are chosen so that upstream radial profiles match with the experimental profiles. As a result, these tools have limited predictive capabilities. Going beyond these mean-field models requires resolving turbulent fluctuations, in a global three-dimensional (3D) geometry, since strong interactions between mean/mesoscale flows and micro-turbulent fluctuations have been evidenced.[7,8] Going for global simulations (in the geometrical sense) also requires paying more attention to the forcing of the turbulence, especially for the charged particle source. In fact, the dominant particle source in the scrape-off layer (SOL)/edge is generally recycling, which occurs close to the divertor plates in diverted plasmas operated in the relevant regimes. Density profiles are thus expected to be mostly flat in the core (excluding pinches and/or neutral beam injection (NBI)-related sources in the plasma core). Compared to a situation where the particle

source is located at the inner boundary condition of the simulation, this affects the pressure gradient in the edge region and thus the drive for interchange turbulence there. Recycling also strongly affects parallel flows in the SOL, especially in diverted configurations.[9]

Over the last decades, considerable simulation efforts have been dedicated to developing the 3D turbulence codes BOUT++,[10] GBS[11] and TOKAM3X[12] to investigate edge turbulent transport. This work relies on TOKAM3X, which includes both open and closed field lines in both limiter and diverted geometries. So far, the isothermal version of TOKAM3X has given new insights into the properties of edge/SOL turbulence, with first simulations in the X-point diverted geometry.[7,8] However, in order to bring the simulations closer to experimental situations in divertor operation, it is necessary to include recycling physics in the models. This is mandatory to address regimes relevant for next-step machines, high recycling regimes, and even detached regimes,[13,14] all the more because experimental evidence points towards changes of transport with the density regimes.[15] Several groups have implemented neutral models in their code, either in 2D[16–18] or 3D codes: a simplified kinetic model in GBS[19] and a fluid model in BOUT++.[20] Moreover, it has been pointed out that additional non-linearities introduced by neutral particle physics lead to additional closure issues in transport codes,[21–23] which are difficult to address quantitatively in mean-field models. Building on the experience gained during the development of Soledge2D-EIRENE, the TOKAM3X code has been fully coupled to the EIRENE Monte Carlo solver.[24] The resulting TOKAM3X-EIRENE code package is first described in this paper, the focus being on code verification.

The rest of the paper is organized as follows: in Section 2, we present the governing fluid equations and the physical setting including description of the geometry. In Section 3, we perform an upstream density scan to recover the density regimes in WEST-like diverted cases. Furthermore, we verify the computations by quantitatively comparing the modified two-point model (2PM) with those from TOKAM3X-EIRENE. The conclusion is provided in Section 4.

2 | THE TOKAM3X-EIRENE CODE

TOKAM3X is a 3D global transport and turbulence fluid code for the edge and SOL plasma of tokamaks, with full geometrical flexibility for the poloidal plasma equilibrium. The particle conservation equation, or continuity equation, is

$$\partial_t N + \vec{\nabla} \cdot [N(u_{||} + \vec{u}_E + \vec{u}^{\,e}_{\nabla B})] = \vec{\nabla} \cdot (D_N \vec{\nabla}_\perp N) + S_N. \tag{1}$$

The parallel momentum conservation equation is

$$\begin{aligned} &\partial_t \Gamma_i + \vec{\nabla} \cdot \left[\Gamma_i \left(\frac{\Gamma_i}{N} \vec{b} + \vec{u}_E + \vec{u}^{\,i}_{\nabla B} + \vec{u}^{\,i}_{curv} \right) + N T_i \vec{b} \right] \\ &= N T_i \vec{\nabla} \cdot \vec{b} - N \nabla_{||} \phi - R_{||} + \vec{\nabla} \cdot \left[D_\Gamma N \vec{\nabla} \left(\frac{\Gamma_i}{N} \right) \right] + \vec{\nabla} \cdot \left(D_N \frac{\Gamma_i}{N} \vec{\nabla} N \right) + S_\Gamma, \end{aligned} \tag{2}$$

where $R_\parallel = 0.71\, N \nabla_\parallel T_e + \eta_\parallel N J_\parallel$ and $E_\parallel = -\nabla_\parallel \phi$. The energy balance for electrons is

$$\begin{aligned} &\partial_t \left(\frac{3}{2} p_e \right) + \vec{\nabla} \cdot \left[\frac{5}{2} T_e (\Gamma_i - J_{||}) \vec{b} + \frac{3}{2} p_e (\vec{u}_E + \vec{u}^{\,e}_{\nabla B}) \right] + \vec{\nabla} \cdot \vec{q}_e \\ &= (J_{||} - \Gamma_i) E_{||} + u_{||i} R_{||} + Q_{||e} + S_{Ee} + \vec{\nabla} \cdot (D_{Te} N \vec{\nabla}_\perp T_e) + \vec{\nabla} \cdot \left(D_N \frac{3}{2} T_e \vec{\nabla}_\perp N_i \right), \end{aligned} \tag{3}$$

while for ions, it is

$$\begin{aligned} &\partial_t \left(\frac{3}{2} p_i + \frac{\Gamma_i^2}{2N} \right) + \vec{\nabla} \cdot \left[\left(\frac{5}{2} p_i \frac{\Gamma_i^2}{2N} \right) u_{||i} \vec{b} + \left(\frac{3}{2} p_i + \frac{\Gamma_i^2}{2N} \right) (\vec{u}_E + \vec{u}^{\,i}_{\nabla B} + \vec{u}_{curv}) \right] + \vec{\nabla} \cdot \vec{q}_i \\ &= N u_{||i} E_{||} - u_{||i} R_{||} + Q_{||i} + S_{Ei} + \vec{\nabla} \cdot (D_{Ti} N \vec{\nabla}_\perp T_i) + \vec{\nabla} \cdot \left[D_N \left(\frac{3}{2} T_i + \frac{\Gamma_i^2}{2N} \right) \vec{\nabla}_\perp N \right] + \vec{\nabla} \cdot \left[\Gamma_i D_\Gamma \vec{\nabla} \left(\frac{\Gamma_i}{N} \right) \right]. \end{aligned} \tag{4}$$

The charge conservation equation is

$$\partial_t W + \vec{\nabla} \cdot \left(W \frac{\Gamma_i}{N} \vec{b} + W \vec{u}_E + W \vec{u}^{\,i}_{\nabla B} \right) = \vec{\nabla} \cdot N (\vec{u}^{\,i}_{\nabla B} - \vec{u}^{\,e}_{\nabla B}) + \vec{\nabla} \cdot (J_{||} \vec{b}) + \vec{\nabla} \cdot (D_W \vec{\nabla} W) + S_W, \tag{5}$$

where $\vec{q_e} = -\chi_{||e} \nabla_{||} T_e \vec{b}$, $\vec{q_i} = -\chi_{||i} \nabla_{||} T_i \vec{b}$, and $W = \vec{\nabla} \cdot \left[\frac{N}{B^2} \vec{\nabla} \phi + \frac{1}{B^2} \vec{\nabla} (N T_i) \right]$. $\vec{b}$ is a unit vector along the magnetic field, and η is the normalized parallel collisional resistivity of the plasma. The energy exchange term between electrons and ions is denoted by $Q_{||i} = -Q_{||e} = 3 \frac{m_e}{m_i} \frac{N}{\tau_e} (T_e - T_i)$. Equations (1)–(5) are, respectively, the particle balance equation, the parallel momentum balance equation, the energy balance equations, and the charge balance equation. The parallel Ohm's law with the electron terms neglected is given by $N_e E_\parallel = -\nabla_\parallel p_e + R_\parallel$. The derivation and normalization were carried out as in Ref. 12. In this work, the

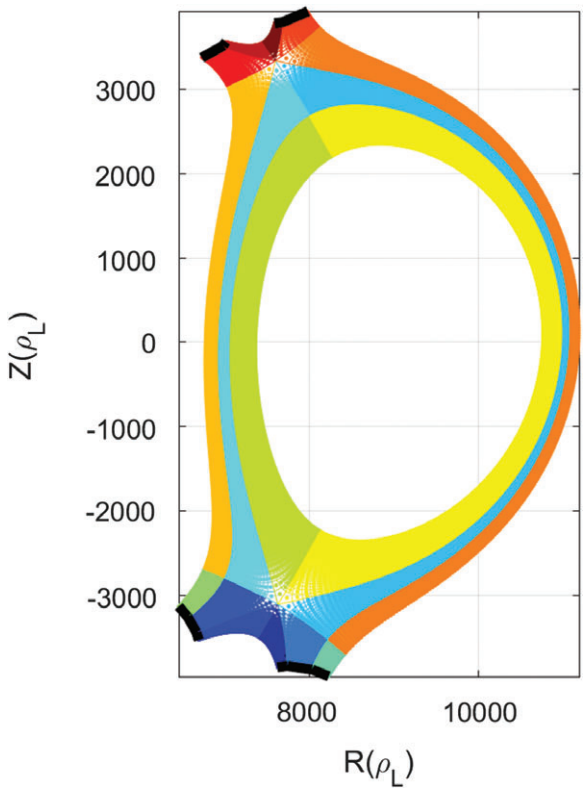


FIGURE 1 The WEST-like mesh grid used in TOKAM3X-EIRENE. Distances are expressed in Larmor radii ρ_L, with $\rho_L = 0.256$ mm here. The colours show the domain decomposition in use, with 16 zones

code is run in the non-isothermal mode, evolving the electron and ion temperatures, which play an important role in recycling physics. The magnetic field is fixed and given as the input of the code, and in the following a full-scale WEST equilibrium is used (Figure 1), together with a simplified wall/divertor target geometry retaining the WEST open divertor feature. The particle source term S_n, parallel momentum source term S_Γ, and energy source term $S_{Ei/e}$ due to interactions with neutrals (atoms and/or molecules) are computed with the EIRENE code.

2.1 | Coupling with the neutral code EIRENE

In order to include neutral physics, the TOKAM3X code has been coupled to EIRENE,[24] which is based on a Monte Carlo process. EIRENE tracks the test particles trajectories (atoms and molecules) and their interactions with the plasma electrons and ions, such as ionization, charge exchange, molecule dissociation, and backscattering of neutrals on the plasma surface. The coupling of the two codes entails data exchange (to be described below), but also physics issues, in particular at the sheath. All the developments available in Soledge2D-EIRENE,[4] in particular to treat the sheath, are available to TOKAM3X-EIRENE since the two codes use the same interface, named STYX. The latter also manages the set-up of EIRENE in coupled runs. In terms of data exchanges, EIRENE takes the TOKAM3X ion flux profiles along the wall (more accurately, at the magnetized sheath entrance) and sample ions hitting the wall accordingly. The latter are then recycled into neutrals (atoms or molecules) according to TRIM databases for backscattering coefficients. The atoms or molecules thus created are followed in the plasma background calculated by TOKAM3X. The resulting particle, momentum, and energy sources are calculated accordingly, and handed back to TOKAM3X. Since TOKAM3X relies on a mixed implicit/explicit scheme, time steps are typically of the order of w_{ci}^{-1} (ω_{ci} is the ion gyro-frequency, i.e., $\sim 10^{-8}$ s), and the EIRENE solver is not called at every time step of the fluid solver ("short cycling"). The STYX interface allows running EIRENE in the time-dependent mode, but this feature is not used here. This means that neutrals do not see any "time horizon", that is, they are tracked during times larger than the time step Δt if they are not ionized or pumped after a time Δt. Note that actually using this feature in turbulent simulations will require careful tuning of the size of the buffer where neutrals reaching the time horizon are stored. Finally, we also mention that while TOKAM3X is a hybrid openmp/MPI code, EIRENE is parallelized with MPI only, a situation requiring further consideration.

2.2 | Geometry and parameters

The TOKAM3X code is designed to run with complex equilibria including X-points. The magnetic field can be expressed as $\vec{B} = F_0 R_0 \vec{\nabla}\phi + \vec{\nabla}\Psi \times \vec{\nabla}\phi$, where F_0 is a total flux number, Ψ is a poloidal flux function, and ϕ denotes the toroidal angle.

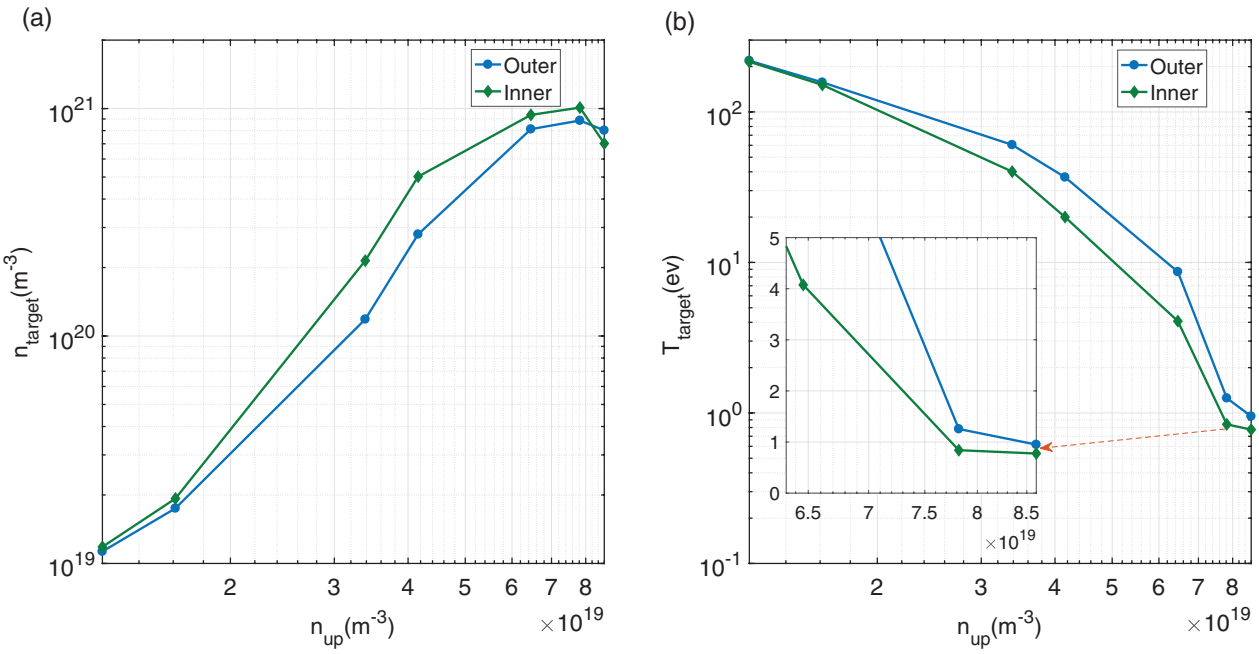


FIGURE 2 (a) Target plasma density n_t and (b) temperature T_t as a function of the outer upstream separatrix plasma density n_{up}, for the inner and outer lower divertor

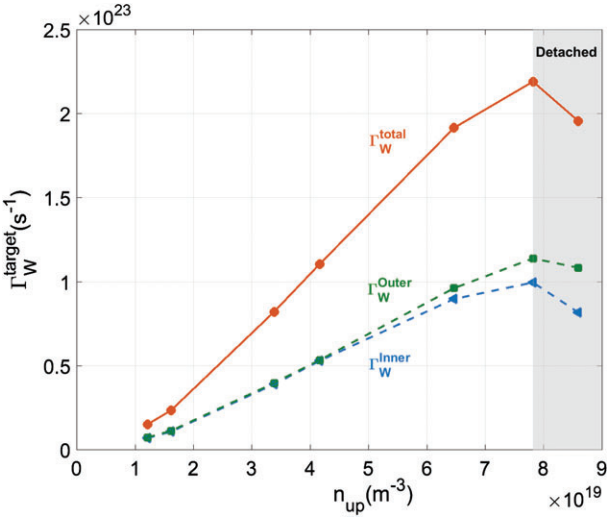


FIGURE 3 Dependence of total recycling flux in the inner and outer lower divertor legs as a function of the outer upstream separatrix density n_{up}

The function Ψ is chosen so as to have a dimensionless magnetic field $B = 1$ at the tokamak axis. The poloidal flux function has been taken from those prepared for the operation of WEST, with two X-points. The minor radius a is equal to $1800\rho_L$, where ρ_L is the ion Larmor radius calculated for the reference parameters used to normalize the plasma fields ($n_0 = 2 \times 10^{19}$ m^{-3}, $T_0 = 50$ eV, and $B_0 = 4$ T). The aspect radio $R/a = 5.1$; that is, the major radius is $R = 2.3$ m. The simulation domain extends from $r_{min} = 0.8a$ in the closed field-lines region to $r_{max} = 1.2a$. The diffusion coefficients for density, parallel momentum, and vorticity are set as $D_N = D_\Gamma = D_W = 0.5$ m^2 s^{-1} (4×10^{-2} in dimensionless units, the normalization factor being $\rho_L^2 \omega_{ci}$, again calculated for the reference parameters). They are uniform in the simulation volume. The parallel resistivity is given as $\eta_{||} = 1 \times 10^{-5} \frac{B_0}{en_0}$. The total input power in the present simulations is 1.4 MW, which is equally shared between ions and electrons, and the power influx at the core edge interface is modelled by a Gaussian source of width $25\rho_L$. In the simulations presented here, there is a particle source at the core, but ultimately the code will be run using a gas puff as primary particle source. The flux of atoms reaching the core edge interface is added to this source, with a uniform poloidal distribution. The outermost magnetic flux surface is assumed to have an effective recycling coefficient (albedo) of $R = 0.99$. Since the focus is on divertor regimes, the code is run with a deuterium plasma without drifts, and the electrostatic potential is calculated in the adiabatic approximation. Furthermore, the code is run in 2D mode (axisymmetry is enforced by conservative averaging in the toroidal direction), hence producing laminar (i.e., non-turbulent) plasma solutions. The effective diffusion coefficients ($D_{N/\Gamma/W}$) modelling turbulent transport in these laminar simulations are prescribed as input data. The code is thus run in exactly the same way as a transport code as a

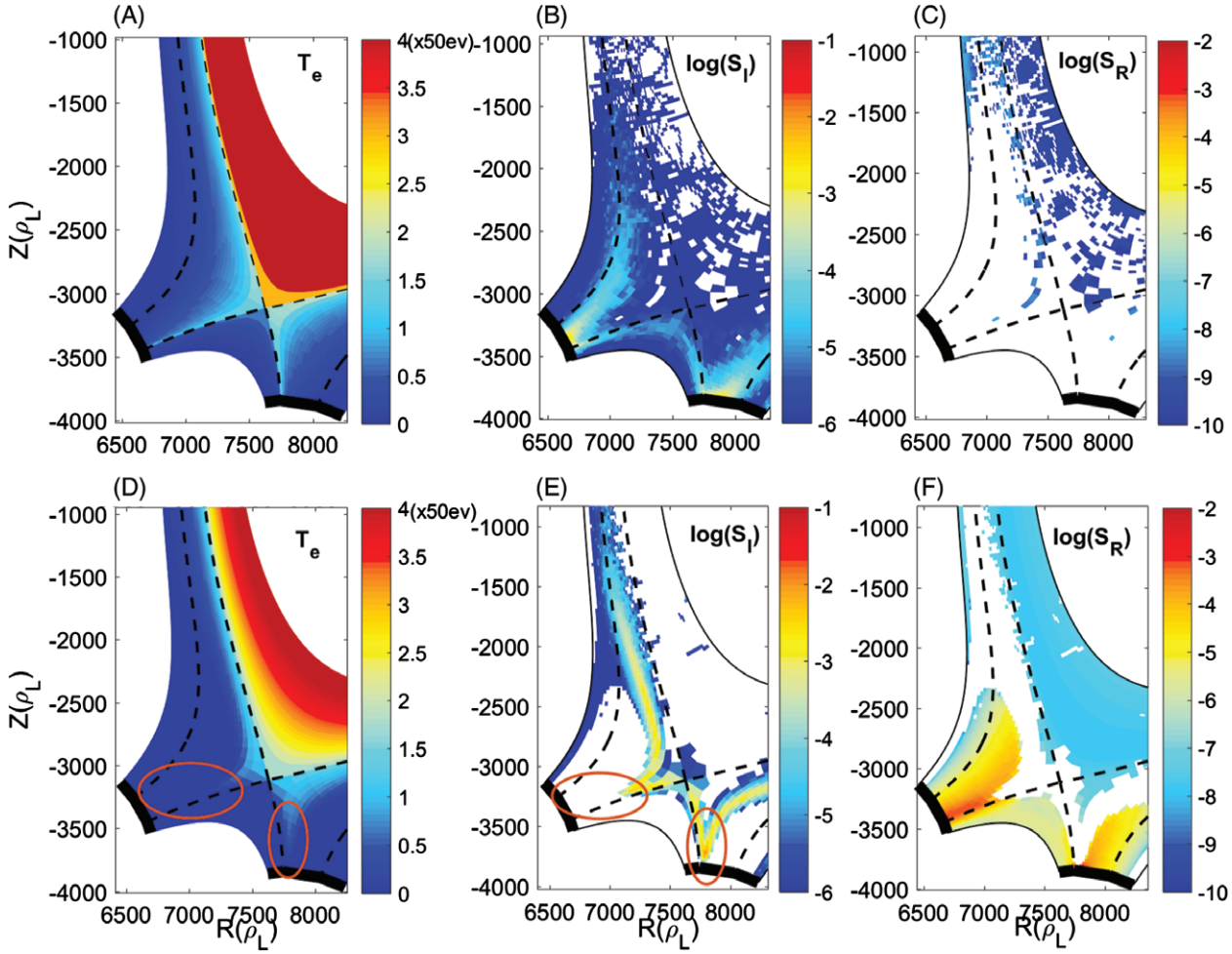


FIGURE 4 TOKAM3X-EIRENE simulation results. Electron temperature (T_e), ionization source (log[S_I]), and recombination sinks (log[S_R]) in the attached regime (a)–(c) and detached regime (d)–(f)

first but key step of the verification procedure. Convergence towards a steady-state solution (in fact, a statistically stationary state due to statistical noise from EIRENE[25]) is assessed by checking for stationarity of all the fields and verifying the global particle and energy balances in the simulations. We thus check that the flux absorbed in the wall ($\phi_{wall} = R(\phi_{D^+} + \phi_D + \phi_{D_2}/2)$) plus the neutral flux at the core edge interface are equal to the influx from the core sustaining the simulation (i.e., the integral of the forcing). As far as energy is concerned, we calculate the energy flux transferred to the wall, which includes the net (i.e., incident minus reflected) kinetic energy flux from both plasma and neutrals, the recombination energy flux on the surface, and the radiated flux, and compare it with the total input power. For simulations presented here, the agreement is within a few percent, both for particles and energy.

3 | RESULTS OF CALCULATION AND MODEL VERIFICATION

The purpose of this section is to show, first qualitatively, that the code correctly reproduces density regimes as the upstream density increases. The scan is made by increasing the particle source in the core from 5.2×10^{19} to 1.3×10^{22} part/s, keeping the power constant at 1.4 MW. Figure 2 shows the evolution of the target density n_t, measured in the outer divertor at the separatrix as a function of upstream mid-plane density. The latter ranges from 10^{19} to 9×10^{19} m^{-3}. Note that, based on Greenwald density considerations, it is not expected that the separatrix density can rise above $\sim 3.5 \times 10^{19}$ m^{-3} in WEST. However, as previously noted, this work is devoted to verifying the code package, so we ignore such concerns. As the upstream density increases, so does the target density n_t in both lower divertor legs, while the target temperature T_t, very close to the upstream temperature T_u at lowest n_u, decreases strongly. For the highest upstream density, the temperature is down to ~ 1 eV, hence corresponding to the onset of detachment. This behaviour is thus qualitatively in line with common wisdom on divertor regimes, showing the transition from the sheath limited to the high recycling and even detached regime. A divertor imbalance is observed, with the inner divertor showing higher density/lower temperature in all the attached cases. The latter results from

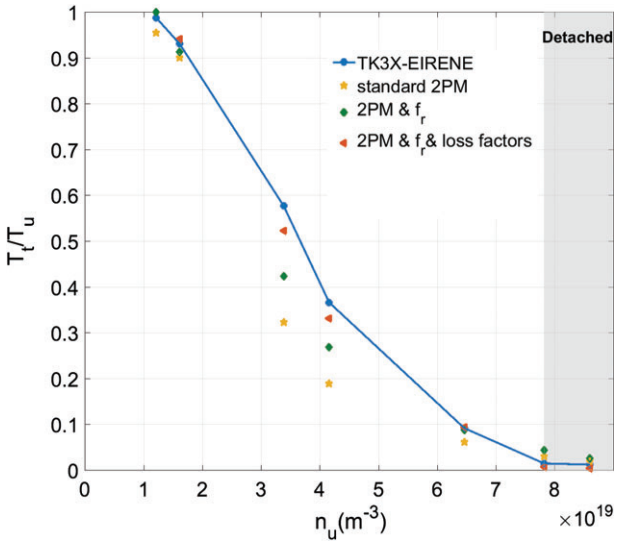


FIGURE 5 Temperature ratio T_t/T_u as a function of the upstream separatrix plasma density n_{up} obtained from the simulation (blue line with circles) compared to the standard (orange stars) and modified two-point model (2PM) scalings (green diamonds and red triangles are, respectively, the results from the modified 2PM [with f_r] and from the modified 2PM [with f_r] taking into account the loss factors)

the low-field-side/high-field-side asymmetry of the magnetic configuration (e.g., Ref. 26). These results are confirmed by the evolution of the total recycling flux in both legs as a function of upstream density, shown in Figure 3, showing a roll-over at a separatrix density of 7.7×10^{19} m^{-3}. With increasing n_{up}, as shown in Figure 4, recombination becomes stronger (Figure 4f) and the cold plasma region in the divertor extends towards the X-point (Figure 4d). Virtually, the divertor is occupied by the cold dense plasma, and the plasma ionization source and the recombination sink are localized close to the X-point and the targets, respectively.

In order to verify whether these trends are quantitatively correct, we compare the results with the 2PM[9] of the SOL in the following. The 2PM connects the upstream and downstream densities and temperatures, using (a) (total) pressure conservation, that is, $n_u T_u = 2 n_t T_t$, (b) parallel energy balance, and (c) sheath physics to express the parallel heat flux as function of the target temperature, namely $q_t = \gamma n_t c_s T_t$. Here, γ is the total sheath heat transmission coefficient, and $c_s = (2T_t/m_i)^{1/2}$ is the sound speed. The total sheath heat transmission coefficient is taken to be $\gamma = 7$, in accordance with the values used in the code. Power balance leads to $T_u^{7/2} = T_t^{7/2} + \frac{7}{2}\frac{q_t L}{\kappa_0}$, where κ_0 is the electron conductivity ($\kappa_0 = 2000$ when electron temperature is expressed in eV) and L the parallel connection length between the upstream location and the target location. The latter is estimated by $L \simeq \pi q R$. Correction factors[9] are usually introduced to account for volumetric momentum (resp. power) losses, f_{mom} (resp. f_{pow}). f_{mom} describes the effects resulting from interactions with neutrals, that is, for momentum losses, friction and volume recombination. The latter can be measured from the simulations. We here assume that all the power is conducted ($f_{cond} = 1$). Further corrections can be made to account for the total flux expansion,[27] leading to the following expression valid when $T_t \ll T_u$ (in fact, $T_t^{7/2} \ll T_u^{7/2}$):

$$\frac{T_t}{T_u} = \left(\frac{7}{2}\frac{q_{||} L}{\kappa}\right)^{8/7} \left(\frac{4\kappa}{7 L \gamma n_u}\right)^2 \left(\frac{\ln f_r}{f_r - 1}\right)^{-6/7} \frac{f_{mom}^2 f_{cond}^{6/7}}{(1 - f_{pow})^2}, \tag{6}$$

where f_r is the total magnetic flux expansion. $q_{||}$ is no longer constant along the flux tube ($q_{||} \propto B$), thus $q_{||} = q_t f_r$. Here, $f_r \simeq 0.7$ so that accounting for flux expansion leads to a correction factor of $\sim$1.4 for T_t/T_u (green diamonds as shown in Figure 5). Note that with reasonable values for our simulations, namely $f_{mom} = 0.8$, $f_{cond} = 1$, and $f_{pow} = 0.2$, we have $f_{mom}^2 f_{cond}^{6/7}/(1 - f_{pow})^2 = 1$. When T_t is not small compared to T_u, we solve for the full model. Comparisons to the 2PM allow checking whether the transition from the sheath-limited regime to the high-recycling regime occurs in the correct range of upstream density n_u, for the power input chosen. The values obtained for T_t/T_u in the simulations (using the outer mid-plane data) are compared with those from the 2PM in Figure 5, and they show good agreement. The 2PM calculations assume here $f_{mom} = 0.8$, $f_{cond} = 1$, and $f_{pow} = 0.1$ in the attached regime, and $f_{mom} = 0.2$, $f_{cond} = 1$, and $f_{pow} = 0.5$ in the detached regime (red triangles shown in Figure 5), in accordance with pressure losses observed in the simulations. The agreement shows that the code predictions for the transition to the conduction-limited and high-recycling regimes are in the correct n_u range.

4 | CONCLUSIONS

The coupling of the TOKAM3X 3D turbulence code with the Monte Carlo code EIRENE has been verified in the laminar mode in X-point geometry, clearing the way for simulations of global electrostatic plasma turbulence including state-of-the-art neutral particle physics. The TOKAM3X-EIRENE verification has been carried out by analysing the results of a density scan, where

standard divertor regimes are observed. The results of the code are consistent with 2PM considerations, for which we considered different refinements. Importantly, the "attached regime" and the "detached regime" are recovered, the total recycling flux along the wall showing a roll-over at very high density case, when the electron temperature in the divertor reaches ∼1 eV.

ACKNOWLEDGMENTS

D.M.F. has been funded through the A*MIDEX project (ANR-11-IDEX-0001-02), the latter being funded by the Investissements d'Avenir French Government programme. This work has been carried out within the framework of the EUROfusion Consortium and French Research Federation for Fusion Studies and has received funding from the Euratom research and training programme 2014–2018 under grant agreement No. 633053. The views and opinions expressed herein do not necessarily reflect those of the European Commission. This work was granted access to the HPC resources of Aix-Marseille Université financed by the project Equip@Meso (ANR-10-EQPX-29-01) of the programme "Investissements d'Avenir" supervised by the Agence Nationale pour la Recherche.

REFERENCES

[1] A. Loarte, B. Lipschultz, A. S. Kukushkin, G. F. Matthews, P. C. Stangeby, N. Asakura, G. F. Counsell, G. Federici, A. Kallenbach, K. Krieger, A. Mahdavi, V. Philipps, D. Reiter, J. Roth, J. Strachan, D. Whyte, R. Doerner, T. Eich, W. Fundamenski, A. Herrmann, M. Fenstermacher, P. Ghendrih, M. Groth, A. Kirschner, S. Konoshima, B. LaBombard, P. Lang, A. W. Leonard, P. Monier-Garbet, R. Neu, H. Pacher, B. Pegourie, R. A. Pitts, S. Takamura, J. Terry, E. Tsitrone, the ITPA Scrape-off Layer and Divertor Physics Topical Group, *Nucl. Fusion* **2007**, *47*, S203.

[2] R. Schneider, X. Bonnin, K. Borrass, D. Coster, H. Kastelewicz, D. Reiter, V. Rozhansky, B. Braams, *Contrib. Plasma Phys.* **2006**, *46*(1–2), 3.

[3] H. Bufferand, B. Bensiali, J. Bucalossi, G. Ciraolo, P. Genesio, P. Ghendrih, Y. Marandet, A. Paredes, F. Schwander, E. Serre, *J. Nucl. Mater.* **2013**, *438*, S445.

[4] H. Bufferand, G. Ciraolo, Y. Marandet, J. Bucalossi, P. Ghendrih, J. Gunn, N. Mellet, P. Tamain, R. Leybros, N. Fedorczak, F. Schwander, E. Serre, *Nucl. Fusion* **2015**, *55*, 053025.

[5] R. Simonini, G. Corrigan, G. Radford, J. Spence, A. Taroni, *Contrib. Plasma Phys.* **1994**, *34*(2–3), 368.

[6] H. Bufferand, G. Ciraolo, P. Ghendrih, Y. Marandet, J. Bucalossi, C. Colin, N. Fedorczak, D. Galassi, J. Gunn, R. Leybros, E. Serre, P. Tamain, *Contrib. Plasma Phys.* **2016**, *56*(6–8), 555.

[7] D. Galassi, P. Tamain, H. Bufferand, G. Ciraolo, P. Ghendrih, C. Baudoin, C. Colin, N. Fedorczak, N. Nace, E. Serre, *Nucl. Fusion* **2017**, *57*, 036029.

[8] P. Tamain, P. Ghendrih, H. Bufferand, G. Ciraolo, C. Colin, N. Fedorczak, N. Nace, F. Schwander, E. Serre, *Plasma Phys. Controlled Fusion* **2015**, *57*, 054014.

[9] P.C. Stangeby, *The Plasma Boundary of Magnetic Fusion Devices*, Institute of Physics Publishing, London **2000**.

[10] B. Dudson, M. Umansky, X. Xu, P. Snyder, H. Wilson, *Comput. Phys. Commun.* **2009**, *180*, 1467.

[11] P. Ricci, F. Halpern, S. Jolliet, J. Loizu, A. Mosetto, A. Fasoli, I. Furno, C. Theiler, *Plasma Phys. Controlled Fusion* **2012**, *54*, 124047.

[12] P. Tamain, H. Bufferand, G. Ciraolo, C. Colin, D. Galassi, P. Ghendrih, F. Schwander, E. Serre, *J. Comput. Phys.* **2016**, *321*, 606.

[13] S. I. Krasheninnikov, A. Kukushkin, W. Lee, A. Pshenov, R. Smirnov, A. Smolyakov, A. Stepanenko, Y. Zhang, *Nucl. Fusion* **2017**, *57*(10), 102010.

[14] B. Lipschultz, B. LaBombard, J. Terry, C. Boswell, I. Hutchinson, *Fusion Sci. Technol.* **2007**, *51*(3), 369.

[15] M. Agostini, J. L. Terry, P. Scarin, S. J. Zweben, *Nucl. Fusion* **2011**, *51*, 053020.

[16] Y. Marandet, P. Tamain, R. Futtersack, P. Ghendrih, H. Bufferand, P. Genesio, A. Mekkaoui, *J. Nucl. Mater.* **2013**, *438*, S518.

[17] N. Bisai, R. Jha, P. K. Kaw, *Phys. Plasmas* **2015**, *22*, 022517.

[18] A. Thrysoe, L. Tophoj, V. Naulin, J. J. Rasmussen, J. Madsen, A. Nielsen, *Plasma Phys. Controlled Fusion* **2016**, *58*, 044010.

[19] C. Wersal, P. Ricci, *Nucl. Fusion* **2015**, *55*, 123014.

[20] J. Leddy, B. Dudson, H. Willett, *Nucl. Mater. Energy* **2017**, *12*, 994.

[21] E. Havlickova, W. Fundamenski, V. Naulin, J. J. Nielsen, S. Wiesen, J. Horacek, J. Seidl, *J. Nucl. Mater.* **2011**, *415*, S471.

[22] Y. Marandet, A. Mekkaoui, D. Reiter, P. Boerner, P. Genesio, J. Rosato, H. Capes, F. Catoire, M. Koubiti, L. Godbert-Mouret, R. Stamm, *Plasma Phys. Controlled Fusion* **2011**, *53*, 065001.

[23] F. Guzman, Y. Marandet, P. Tamain, H. Bufferand, G. Ciraolo, P. Ghendrih, R. Guirlet, J. Rosato, M. Valentinuzzi, *Plasma Phys. Controlled Fusion* **2015**, *57*, 125014.

[24] D. Reiter, M. Baelmans, P. Boerner, *Fusion Sci. Technol.* **2005**, *47*(2), 172.

[25] Y. Marandet, H. Bufferand, G. Ciraolo, P. Genesio, P. Meliga, J. Rosato, E. Serre, P. Tamain, *Contrib. Plasma Phys.* **2016**, *56*, 604.

[26] P. Ghendrih, T. Auphan, B. Bensiali, M. Bilanceri, K. Bodi, A. Bonnement, H. Bufferand, G. Chiavassa, G. Ciraolo, R. Futtersack, C. Guillemaut, Y. Marandet, A. Mentrelli, D. Moulton, A. Paredes, R. Pasquettie, E. Serre, P. Tamain, *J. Nucl. Mater.* **2013**, *438*, S368.

[27] T. Petrie, J. Canik, C. Lasnier, T. Petrie, A. Leonard, M. Mahdavi, J. Watkins, M. Fenstermacher, J. Ferron, R. Groebner, D. Hill, *Nucl. Fusion* **2013**, *53*, 113024.